



**Modelling Long Term Hydraulic Conductivity Behaviour of
Zero Valent Iron Column Tests for PRB Design**

Journal:	<i>Canadian Geotechnical Journal</i>
Manuscript ID	cgj-2015-0453.R1
Manuscript Type:	Article
Date Submitted by the Author:	17-Dec-2015
Complete List of Authors:	Moraci, N.; Mediterranea University of Reggio Calabria, Ielo, Domenico; Mediterranea University of Reggio Calabria, DICEAM Bilardi, Stefania; Mediterranea University of Reggio Calabria, DICEAM Calabrò, Paolo; Mediterranea University of Reggio Calabria, DICEAM
Keyword:	Hydraulic conductivity, zero valent iron, permeable reactive barriers, numerical model



**MODELLING LONG TERM HYDRAULIC CONDUCTIVITY BEHAVIOUR OF ZERO
VALENT IRON COLUMN TESTS FOR PRB DESIGN**

Nicola Moraci^{1*}, Domenico Ielo², Stefania Bilardi³, Paolo S. Calabrò⁴

¹Department of Civil, Energy, Environment and Materials Engineering (DICEAM), Mediterranean University of Reggio Calabria, Reggio Calabria, Italy, nicola.moraci@unirc.it

²Department of Civil, Energy, Environment and Materials Engineering (DICEAM), Mediterranean University of Reggio Calabria, Reggio Calabria, Italy, e-mail: domenico.ielo@unirc.it

³Department of Civil, Energy, Environment and Materials Engineering (DICEAM), Mediterranean University of Reggio Calabria, Reggio Calabria, Italy, stefania.bilardi@unirc.it

⁴Department of Civil, Energy, Environment and Materials Engineering (DICEAM), Mediterranean University of Reggio Calabria, Reggio Calabria, Italy, e-mail: paolo.calabro@unirc.it

*Corresponding author: Nicola Moraci, Via Graziella loc. Feo di Vito 89122, Reggio Calabria, Italy, tel: +39 09651692263 fax: +39 09651692201 e-mail: nicola.moraci@unirc.it

Abstract

In this paper a numerical model to simulate the hydraulic conductivity reduction observed during long term laboratory column tests is proposed. The column tests are carried out in order to study dissolved heavy metals removal by using granular zero valent iron (ZVI). The proposed model is also used to analyse the main causes of hydraulic conductivity reduction observed during laboratory column tests. Expansive iron corrosion, precipitation of reaction products and gas formation are the processes considered in the proposed model. Numerical simulations results show that in order to reproduce the hydraulic behaviour of the experimental systems the change of pores geometry due to expansive iron corrosion and precipitation of reaction products, which determines a possible stop of gas bubbles, should be considered. Furthermore, model results show that only a small percentage of the iron available is corroded during the tests (from 0.4 to 1.9 %). According to the model, the average diameter of gas bubbles that better fit the experimental results is variable between 0.16 and 0.19 mm. While, assuming gas absence (or its possible escape) higher values of iron corrosion rate should be considered in order to fit the experimental results.

Keywords: Hydraulic conductivity, zero valent iron, permeable reactive barriers, numerical model

1. Introduction

1.1 Hydraulic conductivity of Zero Valent Iron Permeable Reactive Barrier

Permeable reactive barriers (PRBs) have gained a considerable importance among the various technologies available to remediate contaminated groundwater, in fact, since the first implementation in the early 1990s, more than 200 PRBs systems have been installed (ITRC 2011). PRBs operate under the natural hydraulic gradient (passive conditions) and therefore it is important to assure, during their service lifetime, that the reactive medium guarantees the preservation of hydraulic conductivity.

Zero valent iron (ZVI) is the most used reactive medium in PRBs thanks to its ability to remove a wide range of groundwater contaminants (Cundy et al. 2008; Fu et al. 2014) as redox-active species (e.g. heavy metals and metalloids) and non-redox sensitive contaminants (e.g. heavy metals like zinc) and to degrade organic compounds (e.g. chlorinated solvents). Other applications of ZVI include stormwater runoff treatment (Rangsivek and Jekel 2005) and water potabilisation at household level (Noubactep 2010).

ZVI can activate different physical and chemical mechanisms for contaminant removal as adsorption, co-precipitation and adsorptive size-exclusion (Noubactep 2011). In particular, ZVI oxidation in aqueous conditions results in formation of iron corrosion products, gas formation (e.g. H_2 in anaerobic conditions), Eh decreases to strongly reducing condition, pH increases with the precipitation of secondary minerals and iron corrosion products. Solids and gas formation depends by many system parameters as iron corrosion rate (O et al. 2009), presence of dissolved chemical compounds (e.g. carbonates, chlorides) (Liang et al. 2000) and groundwater flow velocity (Kamolpornwijit et al. 2003; Kamolpornwijit and Liang 2006; Ruhl et al. 2012a).

Solids and gas formation reduce permeable barrier porosity which results in a decrease in hydraulic conductivity of the reactive medium (Jeen et al. 2006; Jeen et al. 2011; Henderson and Demond 2011). Furthermore, the expansive nature of iron corrosion products (Carè et al. 2008; Zhao et al. 2011), the biological activity, like biofilm growth or biocorrosion (Gu et al. 1999) and the retention

of fine particles, coming from upstream soil, in the PRB pores (i.e. particles clogging) are possible factors that could further contribute to porosity reduction. In order to avoid particles clogging and assure the correct hydraulic behaviour of the barrier in the short term it should be designed according filter criteria (Moraci et al. 2015a).

Literature shows different attempts to understand the phenomena leading to porosity reduction of ZVI-PRB systems. In particular, literature presents studies on the influence on hydraulic conductivity of the expansive nature of iron corrosion products (Carè et al. 2013; Bilardi et al. 2013a; Bilardi et al., 2013b; Noubactep 2013; Domga et al. 2015), of the precipitation of iron corrosion products and secondary minerals (Henderson 2004; Li et al. 2005; Li et al. 2006; Kamolpornwijit and Liang 2006; Komnitsas et al. 2006; O et al. 2009), of colloids (i.e. bentonite and silicium dioxide) precipitation (Courcelles et al. 2008a; 2008b), of gas formation (Mackenzie et al. 1999; Repta, 2001; Zhang and Gillham, 2005; Kamolpornwijit and Liang 2006; Henderson and Demond 2011; Jeen et al. 2012; Ruhl et al. 2012a; Henderson and Demond 2013).

Mackenzie et al. (1999) attributed porosity reduction of the PRB (10% to 15% of the initial porosity) to gas formation. The authors reached this conclusion because the analysis of minerals precipitation, evaluated through aqueous inorganic profiles and analyses of exhausted granular iron, was unable to explain the porosity loss, measured by laboratory tracer tests, in iron column system. Similar results have been reported by Repta (2001) that attributed to gas accumulation a PRB porosity reduction of 20%.

According to Jeen et al. (2006) gas production in ZVI column receiving water contaminated by TCE (Trichloroethylene) without or with CaCO_3 , causes porosity loss variable from 10 to 20 %.

An attempt to evaluate the amount of entrapped gas in column system was performed by Zhang and Gillham (2005) and a porosity reduction of 10% was attributed to this phenomenon; they stated that the non-wetting gas phase accumulates in the largest pores that are the most effective in transmitting water. According to the same authors the porosity loss caused by precipitates formation, as previously noted also in Mackenzie et al. (1999), is not expected to have a major

influence on hydraulic conductivity, being the thickness of the layer of precipitates on iron grains relatively small respect to the diameter of the majority of the pores.

Kamolpornwijit and Liang (2006) have developed a method for measuring gas entrapment in ZVI during column tests; according to their experimental and modelling results, gas venting may be necessary in particular for closed systems. This view has been strongly supported by Henderson and Demond (2011); these authors, through experimental column tests and geochemical modelling, stated that hydraulic conductivity loss was mainly attributable to gas production respect to mineral precipitation.

The same conclusions were reached by Jeon et al. (2012) analyzing the results of theoretical simulations of column studies carried out using a reactive transport model able to combine the effects of both gas bubbles production and secondary mineral formation on the evolution of hydraulic conductivity over time.

Tracer tests and gravimetric measurements indicated the presence of gas entrapped in the columns tests carried out by Ruhl et al. (2012b) using ZVI mixed with respectively sand, gravel, pumice and anthracite.

Henderson and Demond (2013) reported that at the Copenhagen Freight Yard PRB, enough H_2 (g) was produced daily to fill 5% of the PRB pore space. The numerical model developed in their study was able to incorporate the effect of the expansive nature of iron corrosion products and the interaction of gas and solids formation on the hydraulic performance of iron column system.

Notwithstanding the relatively large amount of studies, there are still contrasting views regarding the identification of the main causes of pores clogging in ZVI PRB systems. In fact, when gas production and mineral precipitation are both considered, hydraulic conductivity reduction is, in some cases, mostly attributed to gas formation (Zhang and Gillham 2005; Henderson and Demond 2011; Jeon et al. 2012), while, in other cases, it is mostly attributed to mineral precipitation (Kamolpornwijit et al. 2003, Kamolpornwijit and Liang 2006). This mismatch could be mostly attributable to the possible differences in the extent of solids and gas formation due to the dissimilar

conditions (e.g. of flow rate and chemical composition of groundwater, oxic/anoxic conditions) of the PRB systems considered in the different studies.

Since the grain size distribution of the reactive medium is chosen according filter criteria, the behaviour of a PRB can be simulated through laboratory experiments (column tests mainly) carried out using conditions of flow rate, temperature and groundwater chemical composition as much similar as possible to those expected in situ (Moraci et al. 2014a). These studies provide useful information for understanding only the early lifetime of the treatment system (maximum up to 2 years) otherwise experiments having the same lifetime of the barrier, usually more than 10 years, should be necessary. For this reason numerical models able to predict the long term behaviour of the barrier can represent an important tool for its design.

However, model calibration should always be based on the results of lab-scale experiments performed, as already mentioned, trying to reproduce site - specific conditions (Carniato et al. 2012). Often, for practical reason, lab-scale experiments are accelerated by increasing the flow rate respect to field conditions, unfortunately this practice considerably affects the reliability of the obtained test results (Bilardi et al. 2012; Moraci et al. 2014a). This fact further augments the importance of the availability of reliable theoretical models for the simulation of the long-term behaviour of a PRB.

In this paper, a numerical-statistical geometrical model simulating hydraulic conductivity reduction observed in ZVI laboratory column tests, using either nickel alone or nickel, zinc and copper as contaminants, is proposed. The model takes into account iron corrosion, including its expansive nature, the synthesis and precipitation of iron/contaminants compounds and gas formation.

The goal of this study is to understand by means of the proposed model, the phenomena causing the major decrease of hydraulic conductivity observed in ZVI systems. Moreover, the model could be used during design phase, together with column tests, to forecast the long term behaviour of the ZVI PRB in terms of both hydraulic conductivity and average iron corrosion rate.

1.2 Contaminants and iron corrosion products in ZVI systems

Ni removal by ZVI has been mainly attributed to adsorption, co-precipitation and adsorptive size-exclusion (Calabrò et al. 2012; Dries et al. 2005; Bartzas et al. 2006; Bilardi et al. 2013a), the possibility of a spontaneous electrochemical cementation process between Ni and ZVI is less favoured because, the standard redox potential of the couple $\text{Ni}^{2+}/\text{Ni}^0$ is only slightly higher than that of $\text{Fe}^{2+}/\text{Fe}^0$.

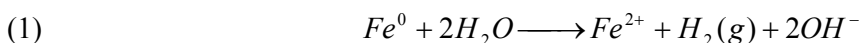
Cu removal is mainly attributed to the reduction of the oxidised form of the contaminant, Cu^{II} , to Cu^0 onto the iron surface (cementation process) but also to adsorption and coprecipitation on iron corrosion products (Komnitsas et al. 2006; Moraci et al. 2011; Rangsviek and Jekel 2011; Bilardi et al. 2015).

Respect to Cu and Ni the reduction of Zn by ZVI is excluded since the standard redox potential of the couple $\text{Zn}^{2+}/\text{Zn}^0$ is lower than that of $\text{Fe}^{2+}/\text{Fe}^0$ and therefore its removal is due to the other mechanisms activated by ZVI (Bartzas et al. 2006; Rangsviek and Jekel 2011; Dries et al. 2005; Bilardi et al. 2015).

In the model proposed in the paper, the final volume of precipitates, generated during contaminant removal, was calculated knowing the mass of contaminant removed at the end of the tests (derived by a mass balance) and hypothesizing that Ni precipitates in the system as trevorite $\text{Ni}(\text{Fe}^{3+})_2\text{O}_4$, (density equal to 5.165 g/cm^3) as detected in previous studies (Moraci et al. 2011), Cu precipitates as Cu^0 (density equal to 8.92 g/cm^3) and Zn as $\text{Zn}(\text{OH})_2$ (density equal to 3.053 g/cm^3). It was hypothesized that the volume of precipitates increases linearly over time up to the final value.

Iron corrosion products were detected in a previous study (Bilardi et al. 2013c) through X-ray photoelectron spectroscopy analyses, and were identified goethite, hematite, and magnetite.

In anaerobic condition iron corrosion results in the formation of hydrogen according the following equation:



In this reaction, 1 mole of hydrogen gas is generated for every mole of iron corroded by water. Hydrogen produced during column tests carried out using granular ZVI can be divided into three phases: gas phase, aqueous phase and solid phase (entrapment of hydrogen in the iron) (Reardon 1995, 2005; O et al. 2009). According to literature studies (O et al. 2009), H_2 in the gas phase is about 65% of the total and this value was assumed in the proposed model.

Knowing the mass of ZVI, used in the column experiments, and the average iron corrosion rate, hydrogen production is calculated according to equations 1 and the ideal gas law. Production of hydrogen volume is evaluated considering the evolution of the absolute pressure variable approximately between 1 and 2 atm (pressure at the beginning and at the end of test compatible with the used peristaltic pump).

The average diameter of gas bubbles, depends by a number of factors (e.g. pressure and temperature) and it is considered a model calibration parameter.

2. Column tests

2.1 Materials and contaminated solutions

The used ZVI is of the type FERBLAST RI 850/3.5, distributed by Pometon S.p.A., Mestre - Italy. The material contains mainly iron (> 99.74 %). It is characterized by uniform grain size distribution (Figure 1). The mean grain size (d_{50}) is about 0.5 mm and the coefficient of uniformity (C_u , ratio between the diameters corresponding to 60 and 10 % finer in the grain size distribution = d_{60}/d_{10}) is 2. The particle density of the reactive material is equal to 7.87 g/cm^3 . The granular ZVI was packed in the columns obtaining a porosity of about 47 %.

The contaminated aqueous solutions were prepared by dissolving nickel(II) nitrate hexahydrate, copper(II) nitrate hydrate and zinc(II) nitrate hexahydrate obtained from Sigma-Aldrich (Sigma - Aldrich purity 99.999) in distilled water.

2.2 Test method and experimental program

The column tests results, used in this paper as benchmark with model results, are described in detail elsewhere (Moraci and Calabrò 2010; Bilardi et al. 2015; Moraci et al. 2014a). The tests were performed using laboratory scale polymethyl methacrylate (PMMA—Plexiglas™) columns (50 cm long, 5 ± 0.1 cm inner diameter) equipped with several sampling ports located at different distances from the inlet. The influent solution was pumped upwards using a precision peristaltic pump (Ismatec, ISM930). During column tests hydraulic conductivity was determined, using either the falling-head or constant-head permeability methods as appropriate (Head and Keeton 2008).

The proposed numerical statistical-geometrical model is used to simulate the hydraulic behavior observed in different column tests, whose results in terms of removal efficiency and hydraulic behavior are discussed in details in Moraci et al. (2014a) for Test A, B, D, F and G, in Moraci and Calabrò (2010) for Test C and in Bilardi et al. (2015) for Test E. The main parameters of the modelling column tests are summarized in Table 1.

The three different Darcy velocities used correspond, for Tests A (and Test D), B (and Tests F and G) and C (and Test E), to a flow rate in the column of 0.1, 2.5 and 0.5 ml/min. Since the volume occupied by the reactive medium was lower than the total volume of the column, inert material (washed quartz gravel) was used to fill the remaining space. The aqueous concentrations of Ni, Cu and Zn were measured by Atomic Absorption Spectrophotometry (AAS - Shimadzu AA – 6701F) using conventional Standard Methods (APHA 2005).

3. Proposed theoretical model

The proposed numerical model is derived by Simulfiltr, a new theoretical method developed to simulate the filtration process inside granular soils in order to evaluate their internal stability (Moraci 2010; Moraci et al. 2012a, 2012b, 2012c, 2014b, 2015b).

The new proposed model also simulates the gas bubble movement, inside the granular reactive medium; the positions of its grains are considered fixed over time and its porosity varies because of i) expansion of iron grains due to corrosion, ii) precipitation of iron/contaminant compounds and iii) entrapment of gas bubbles.

The main assumptions of the model are:

- a) The particles clogging is negligible (the PRB is designed according filter criteria);
- b) ZVI granular particles are spherical;
- c) Gas bubbles are spherical (this is perfectly adherent to reality due to the tendency of the fluid to reduce surface energy and in fact the spheres have the smallest surface area of any shape, for a given volume);
- d) coalescence of the bubbles negligible since their detachment from ZVI surface until their stop due to the presence of constrictions (i.e. the narrowest part of the pore) smaller than the size of the bubble.

3.1 Reactive medium schematization

The reactive medium composed by ZVI granular particles is represented by a sequence of parallel layers, placed upon each other at a distance, in the direction of hydraulic flow, equal to the ZVI mean grain size (Figure 2). The constrictions are created by the contact of four ZVI particles in different combinations (Moraci et al. 2012a, 2012b).

In order to simulate the randomness of bubbles and constrictions positions, a sampling stochastic method on the cumulated numerical distribution of both the number and size of constrictions and bubbles is applied (Moraci et al. 2012a).

The constrictions grain size distribution is obtained applying the geometric stochastic method proposed by Silveira (1965) and Silveira et al. (1975) to the ZVI grain size distribution.

The ZVI numerical percentage grain size distribution, characterized by D_i and ΔP_{ni} values, is obtained from the soil weight percentage grain size distribution discretized by N diameter D_i (Figure 3) considering the following relation (Musso and Federico 1983):

$$(2) \quad \Delta P_{ni}(D_i) = \frac{\frac{\Delta P_{mi}}{D_i^3}}{\sum_{i=1}^N \frac{\Delta P_{mi}}{D_i^3}}$$

where $\Delta P_{mi}(D_i)$ is the weight frequency of the particle fraction with average diameter D_i and $\Delta P_{ni}(D_i)$ is the numerical frequency of the particle fraction with average diameter D_i .

All possible set of four particles diameters (D_i, D_j, D_k, D_m) are taken into account. The total number of these ones represents the $C_{N,4}^r$ combination number with repetition of the N diameters (D_1, D_2, \dots, D_N) taken four at a time. The value of $C_{N,4}^r$ is equal to Silveira et al. (1975):

$$(3) \quad C_{N,4}^r = \frac{(N+3)!}{4!(N-1)!}$$

For each of the $C_{N,4}^r$ set of particles, given that the grain size distribution of ZVI sample is uniform, it is possible to consider the group equivalent that consists of 4 particles with a diameter D_{mean} equal to volume-weighted mean diameter of the four particles diameters (D_i, D_j, D_k, D_m) and the constriction size is chosen equal to the circle having diameter (Figure 4):

$$(4) \quad D_v = (\sqrt{2} - 1)D_{mean}$$

The ΔP_v likelihood that a void of fixed diameter D_v is formed depends on the likelihood that four particles of D_i, D_j, D_k, D_m diameters are at the same time in contact. The ΔP_v value is expressed as function of the $\Delta P_{ni}, \Delta P_{nj}, \Delta P_{nk}, \Delta P_{nm}$, likelihood values associated respectively to the D_i, D_j, D_k, D_m diameters of the particles as follows:

$$(5) \quad \Delta P_v(D_v) = \frac{4!}{r_i!r_j!r_k!r_m!} \Delta P_{ni}^{r_i} \Delta P_{nj}^{r_j} \Delta P_{nk}^{r_k} \Delta P_{nm}^{r_m}$$

In the (4) expression the r_i, r_j, r_k, r_m terms represent the times number that the particles of D_i, D_j, D_k, D_m diameters take part in the set of four numbers. The addition $r_i + r_j + r_k + r_m$ is equal to 4.

The cumulated frequencies $\sum_{i=1}^{C_{N,4}^r} \Delta P_{v,i} = P_v$ are calculated after that the $C_{N,4}^r$ couples of values in terms of $D_v, \Delta P_v$ are known, named constriction size distribution (Figure 5).

The applied procedure can be described as follows (Moraci et al. 2012a):

1. The graph of the cumulated numerical percentage distribution of the bubbles sizes is drawn (this distribution is calibrated in order to obtain the best fit with experimental results from column tests).
2. The graph of the cumulated numerical percentage distribution of the constrictions sizes is drawn.
3. A random number with uniform distribution between zero and one (i.e. using the “Cristoforo Colombo” Matlab™ generator, The MathWorks, Inc., Natick, Massachusetts) is generated.
4. The so-found number is reported on the vertical axis, projected horizontally on the curve, and the point intercepted on the curve is then projected vertically on the x axis (Figure 6).
5. The so-found corresponding abscissa value is taken as one of the values for the bubble diameter or for the constriction diameter that can be included in the layer.

It is assumed that H_2 bubbles develop simultaneously in the whole reactive medium.

3.2 Simulation of gas bubbles movement

The simulation of gas bubbles movement is performed by comparing each bubble contained in the i layer with the constrictions contained in the next $i + 1$ layer (Figure 7, where s is layer number).

The steps of the simulation algorithm, are the following:

1. Time $t=0$
2. Choice of the generic bubble having diameter equal to D_b , in the i layer.
3. Comparison of the bubble size, D_b , with the size D_v of the four constrictions corresponding in the $i + 1$ layer (Figure 7).

4. If the bubble is smaller than one of the four constrictions, it goes into the next layer otherwise it is stopped in the i layer (Figure 8).
5. Repetition of the previous steps for all the bubbles contained in the i layer.
6. Passage to the next $i + 1$ layer and repetition of steps 1–4.
7. Determination of the arrested bubble in all layers and update of porosity, specific area and the ratio k/k_0 between the hydraulic conductivity k at the time t and the one k_0 at the initial time t_0 of the system.
8. Increase of time Δt (equal to test duration divided by 200) and calculation of volume occupied by iron corrosion products and contaminant precipitates and consequently of the dimension of the new constrictions.
9. Repetition of steps 1–7
10. For each $t < t_{end}$ (end of the test) the ratio between actual and initial permeability are reported.

3.3 Iron expansion volume determination

Literature (Pilling and Bedworth 1923; Anstice et al. 1993; Carè et al. 2008) shows that the volume of the ZVI after corrosion is higher than that of the original metal. The ratio between the volume of corrosion products ($V_{iron_corrosion_products}$) and volume of iron consumed in the corrosion process ($V_{iron_corroded}$) called “rust expansion coefficient” (η) was introduced by Carè et al. (2008) (eq. 6):

$$(6) \quad V_{iron_corrosion_products} = \eta \cdot V_{iron_corroded}$$

η values are in the range 2.08 - 6.4 (Carè et al. 2008; Zhao et al. 2011), the lowest value corresponds to Fe_3O_4 as only corrosion product (anoxic conditions) and the largest one to $Fe(OH)_3 \cdot 3H_2O$ (oxic conditions) (Noubactep 2013).

Therefore the iron expansion volume (V_{exp}) can be calculated according equation 7:

$$(7) \quad V_{exp} = (\eta - 1) \cdot V_{iron_corroded}$$

The amount of $V_{iron_corroded}$ was determined through the iron corrosion rate ($Iron_corrosion_rate$) considered a model calibration parameter. This parameter as shown in literature (Ruhl et al. 2012a; O et al. 2009; Triszcz et al. 2009; Velimirovic et al. 2014), strictly depends by the intrinsic reactivity of Fe^0 , the experimental conditions (e.g. hydrodynamic conditions, massic flow of contaminants, pH, dissolved O_2 , nature and extent of contamination), effective stresses and filter dimension. It is assumed that ZVI expansion is uniform for each particle (particles remain spherical).

The amount of $V_{iron_corroded}$ [cm^3] was evaluated through equation 8:

$$(8) \quad V_{iron_corroded} = \frac{PM_{ZVI}}{\rho_{ZVI}} \cdot t \cdot Iron_corrosion_rate \cdot M_{ZVI} \cdot 10^{-6}$$

Where PM_{ZVI} and ρ_{ZVI} are the respectively the molecular weight [55.8 g/mol] and density [7.87 g/cm³] of the ZVI, t is the time [day], M_{ZVI} is the mass of ZVI [g].

3.4 Hydraulic conductivity and porosity reduction calculation

Based on the Kozeny-Carman equation (Bear 1972), the hydraulic conductivity k can be calculated as:

$$(9) \quad k(t) = T_o \frac{n(t)^3}{(1-n(t))^2 M_s(t)^2}$$

Where $n(t)$ is the porosity at time t , $M_s(t)$ is the specific surface area at time t (area per unit volume of particles) and T_o is a tortuosity parameter.

Considering the set i -th of 4 particles of diameter D_{mean} (Figure 8) and defining N_p equals at the number of the set i -th of particles contained in the schematization of the ZVI sample, the porosity of the reactive medium at time t is given by equation 10:

$$(10) \quad n(t) = \frac{\sum_{i=1}^{Np} V_{v0i} - \sum_{i=1}^{Np} V_{expi}(t) - V_{prec}(t) - V_{bub}(t)}{\sum_{i=1}^{Np} V_{ti}}$$

Where V_{v0i} is the initial volume of the void in the set i -th; $V_{expi}(t)$ is the iron expansion volume in the set i -th (eq.6); $V_{prec}(t)$ is the volume of contaminant precipitates at time t in the overall reactive medium; $V_{bub}(t)$ is the volume of gas bubble arrested at time t in the overall reactive medium (since gas bubbles cannot be crossed by the flow they are considered as a solid having a own volume and surface); V_{ti} is the total volume of the set i -th.

The volume overlapping (Figure 9) is supposed to be redistributed upon free surfaces.

Surface at time t is calculated through equation 11:

$$(11) \quad S(t) = \sum_{i=1}^{Np} S_{0i} + \sum_{i=1}^{Np} S_{expi}(t) - \sum_{i=1}^{Np} S_{overlapi}(t) + S_{prec}(t) + S_{bub}(t)$$

Where S_{0i} is the surface of the set i -th at time $t = 0$; $S_{expi}(t)$ is the increase of the ZVI surface due to iron corrosion products in the set i -th at time t (included the overlapping surface); $S_{overlapi}(t)$ is the overlapping surface in the set i -th at time t (Figure 9) including the variation of the surface due to the volume overlapping redistributed; $S_{prec}(t)$ is the surface of contaminant precipitate at time t in the overall reactive medium; $S_{bub}(t)$ is the surface of the arrested bubble at time t in the overall reactive medium.

The specific surface $M_s(t)$ can be determined from (12):

$$(12) \quad M_s(t) = \frac{S(t)}{V_s(t)}$$

Where $V_s(t)$ is the overall reactive medium volume at time t including the volume of the precipitates and that one of the arrested gas bubble:

$$(13) \quad V_s(t) = \sum_{i=1}^{Np} V_{s0i} + \sum_{i=1}^{Np} V_{expi}(t) + V_{prec}(t) + V_{bub}(t)$$

Where V_{s0i} is the initial solid volume of the set i -th at time $t=0$;

The presence of precipitates on ZVI surface causes a reduction of the pores constrictions size; this phenomenon was taken into account by means of two different methods:

1. Considering a redistribution of the volume of precipitates on the ZVI expanded surface;
2. Considering the random formation of spherical particles of precipitates, on ZVI surface, whose average diameter is a parameter of the model variable between 0.01 and 0.1 mm, a range that can be considered realistic comparing at the mean particle diameter of the grain size distribution equals to 0.5 mm.

In figure 10 the ZVI particle, its volumetric expansion and the contaminant precipitation schemes are shown.

In the second method the value of each constriction diameter $D_v(t)$ (Figure 11) decreases with time following equation 14:

$$(14) \quad D_v(t) = 0.414D_{mean}(t) - D_{prec}$$

Where $D_{mean}(t)$ is the mean diameter of four ZVI particles which varies with time; D_{prec} is the average diameter of precipitates (variable between 0.01 – 0.1 mm).

In the simulations the difference in the outputs determined by means of the two methods is negligible and therefore the outputs related to the first method are shown.

3.5 Model parameters

The model aims at calculating the variation with time of the hydraulic conductivity $k(t)$. The ratio $k(t)/k_0$ depends on the variation of different parameter (i.e. porosity, particles and bubbles specific surface, size of constrictions between iron grains and gas bubbles).

In order to simulate long term hydraulic behaviour of ZVI column tests two approaches are used.

Approach 1

In this approach the effect of the expansive iron corrosion (i), of the expansive iron corrosion and precipitation of reaction products (ii) and of these two processes with gas formation (iii) are the processes considered in the model.

In this simulation approach the calibration parameters are the iron corrosion rate, the average gas bubbles diameter and the standard deviation σ of its frequency distribution.

The discrete frequency distribution of the bubbles diameters is approximated by a Gaussian distribution characterized by a mean " μ ", calibrated in order to fit the experimental results, variable in the range between 0.165 mm and 0.175 mm for all tests carried out using monocontaminant solution, and equal to 0.190 mm for the test E carried out using pluricontaminant solution.

Approach 2

In this approach gas absence (or its possible complete escape) is assumed and the only processes considered are: the expansive iron corrosion (i) and the expansive iron corrosion with precipitation of reaction products (ii). In this case the calibration parameters is only the iron corrosion rate.

In both simulation approaches, the parameter η is assumed equal to 2.37 which is the average value calculated among the three species detected during experimental activity (see par. 1.2) i.e. Goethite ($\eta = 2.91$), Hematite ($\eta = 2.12$) and Magnetite ($\eta = 2.08$) (Carè et al. 2008).

An initial ZVI specific surface area equal to 0.17 m²/g (Bilardi et al. 2013c) is used in the model.

Actually it was necessary to simulate only the behaviour of the first 1.5 cm of reactive medium (30 layer x 30 rows x 30 columns) because clogging is usually observed only at the entrance zone of ZVI systems (Mackenzie et al. 1999; Wilkin et al. 2003; Kaplan and Gilmore 2004; O et al. 2009; Noubactep 2013).

The input parameters used in both simulation approaches are summarized for all column tests in table 2. Calibration parameters of the two simulation approaches are reassumed in table 3 and 4

respectively. The iron corrosion rate evaluated by the model should be considered an average value, since it could reduce over time (Parbs et al. 2007; O et al. 2009).

4 Results and discussion

Figures 12 – 18 show the variation of hydraulic conductivity normalized respect to the initial value, during the column tests (from A to G). In the figures are showed the values determined by means of permeability test (full rhomboid symbols) and the results obtained using the new proposed model according to the two different approaches.

In particular, figures 12a - 18a show results obtained with the simulation approach 1 while figures 12b-18b show those obtained with the simulation approach 2.

According to the simulation approach 1 (Figures 12a - 18a) when only ZVI expansion is considered (dotted lines) the variation of the ratio k/k_0 is linear with time and does not fit the observed hydraulic conductivity reduction (full rhomboid symbols).

When ZVI expansion and precipitates formation are considered (dashed lines) the variation of k/k_0 profile is linear with time (a slightly greater slope) and also in this case model results are not satisfactory.

When ZVI expansion, mineral precipitation and gas formation are considered (solid lines) the model is able to match in a more satisfactory way the hydraulic conductivity reduction observed in the column tests. A similar result can be obtained considering only iron corrosion products and gas formation due to the slight influence of precipitates derived by contaminant removal on the results. The negligible volume of these compounds, compared to the volume of voids of the reactive medium, and the consequently negligible impact on the hydraulic conductivity loss observed in ZVI systems, was also confirmed in literature by Parbs et al. (2007); Henderson and Demond (2011) and Jeen et al. (2006, 2012).

The new proposed model is able to match the sudden decrease of hydraulic conductivity, that is often observed in column tests. This behaviour according to model results could be due to gas

stopping due to a reduction in constriction size (with dimension lower than average gas bubble diameter).

The hydraulic conductivity loss due to gas entrapment validates the idea expressed in literature by Carè et al. (2013) .

Based on numerical analyses, the parameter which main influences model results is the iron corrosion rate, therefore it is possible to infer that the hydraulic performance of a ZVI-system is strictly dependent by the intrinsic reactivity of iron which is function of iron material composition, particle size, temperature, and water composition (Reardon 1995; Weber et al. 2013).

In the case of the analysed column tests, the value of iron corrosion rate is influencing by only water composition and flow rate (since ZVI type and particle size are the same and temperature variation is slight). Therefore, according model results clogging occurs faster for higher values of the iron corrosion rate, this behaviour was also remarked in literature by O et al. (2009).

According to numerical model results, a comparison, between tests carried out with the same flow velocity (see Tests A and D or Tests B, F and G), points out as higher values of the initial contaminant concentration decreases the iron corrosion rate. Therefore the hydraulic conductivity loss is faster using lowest values of nickel concentration. These results could be due to ZVI oxidation, by the solution, which is likely more relevant at lower values of Nickel concentration. A similar behavior was observed by Zhang and Gillham (2005), that found a lower porosity loss in a column test using distilled water rather than using water contaminated by TCE. Another possible explanation could be attributed to nitrate, whom presence, which increases with nickel concentration (nickel(II) nitrate hexahydrate was the reagent used in the experiments), has shown to slow down ZVI corrosion (Farrell et al. 2000; Henderson and Demond 2007).

On the contrary, considering the same contaminant concentration (e.g. Tests A and B or Tests D and F), numerical model results indicate a greater gas production or equivalently an increase of the iron corrosion rate with the increase of flow rate. This behavior was also observed in literature by Kamolpornwijit and Liang (2006) according to the free gas volumes collected from two field

columns. In that study the volumes of the gas collected reached a maximum of ~660 ml/d in the high-flow column and of 50 ml/d in the low-flow column.

According to model results the extent of ZVI depletion α (Carè et al. 2013; Noubactep 2013), calculated through equation 15, varies from only 0.4 % to 1.99 % (see Table 5) this means that only a small percentage of the iron available were actually corroded.

$$(15) \quad \alpha = \frac{\frac{PM_{ZVI} \cdot Iron_corrosion_rate \cdot M_{ZVI} \cdot t \cdot 10^{-6}}{\rho_{ZVI}}}{\frac{M_{ZVI}}{\rho_{ZVI}}} = PM_{ZVI} \cdot Iron_corrosion_rate \cdot t \cdot 10^{-6}$$

This is similar with the results reported in Carè et al. (2013) by means of a mathematical modeling based on mass conservation equations. According to the authors very low values of α (ranging from 0.01 % to 0.06 %) can be expected when H₂ remain in the system. On the contrary, under the hypothesis that H₂ is free to escape, values of α variable from 16 % to 98 - 100% can be found (Carè et al. 2013).

A similar behaviour is also observed by the model using the simulation approach 2 and assuming the absence of H₂ production (or the possible escape). Model results obtained for Tests A - G (Figures 12b - 18b), show as in order to fit the experimental results (full rhomboid symbols), assuming the absence of gas (or its possible escape), higher values of iron corrosion rate should be considered (Table 4). As previously observed, considering only ZVI expansion (dashed lines) or both ZVI expansion and precipitates formation (dotted lines) the difference is negligible due to the slight influence of mineral precipitates derived by contaminant removal. In this case the values of α obtained vary from 4.2 to 43.9 % (Table 5). It is also possible to point out the linear relationship between the porosity loss and α (Figure 19) until a value almost constant of α in proximity of clogging (porosity loss > 90 %) is achieved. In this condition the extent of ZVI depletion ranging from 33.7 to 43.9 %.

Since the values of iron corrosion rate, considered in the simulation approach 2, are significantly higher than those found in literature and since gas escape in the actual column tests is rather difficult, the presence of gas bubbles is likely to play an important role.

According to the results presented in this paper, in order to allow a better use of ZVI in terms of both remediation efficiency and cost effectiveness, on a real PRB, it could be useful:

- favouring the natural venting of the gas produced as proposed also in literature (Kamolpornwijit and Liang 2006; Henderson and Demond 2011);
- using technologies such as sonication to periodically fragment gas bubbles in order to promote their exit from the system;
- using a porous supporting material (e.g. pumice) to store gas and precipitates.

5 Conclusions

In this study, the results of hydraulic conductivity variation observed in column tests, carried out using granular ZVI for dissolved nickel removal, and for dissolved nickel-copper-zinc removal, are simulated through a numerical-statistical geometrical model, implemented in order to simulate filtration process and to investigate the main causes of the hydraulic conductivity decline of ZVI systems over time.

According to model results, volumetric expansion of iron and mineral precipitation phenomena can contribute to a change in the geometry of the pores which determines a possible stop of generated gas bubbles. According to the model, the average diameter of gas bubbles at the time of their detachment from the iron particle surface, is variable between 0.16 and 0.19 mm. Model results show also that in this conditions only a small percentage of the iron available is corroded (from 0.4 to 1.99 %).

On the contrary assuming gas absence (or its possible complete escape) in order to fit experimental data higher values of iron corrosion rate should be considered. In this case in proximity of clogging

(porosity loss greater than 90 %) a higher extent of ZVI depletion ranging from 33 to 43 % was evaluated.

For further validation of the model in presence of gas bubble, other researches are necessary in order to exactly determine the dimension and distribution of the bubbles during the test that depend on the temperature, surface tension, pH of the contaminant liquid and on the pressure.

Since the duration of laboratory column experiments is usually limited to a few months, the model could be used in a predictive manner in order to estimate more precisely the hydraulic conductivity variation and thus the longevity of the ZVI system in the long term.

One of the major issues related to the use of pure ZVI is maintaining the hydraulic conductivity over time. An established way to overcome this problems is the use of granular mixtures between ZVI and other inert and/or porous materials (e.g. sand, pumice), for this reason in the future the model will be extended to bi-component systems (e.g. ZVI-Pumice, ZVI-sand).

Acknowledgements

This research was funded by the MIUR Project PON01_01869 TEMADITUTELA. Experimental data are properly cited and referred to in the reference list, they are also available on request (nicola.moraci@unirc.it).

References

- Anstice, C., Alonso, C., and Molina, F.J. 1993. Cover cracking as a function of bar corrosion: Part I-Experimental test, *Materials and structures*, **26**(8), 453-464.
- APHA, AWWA, WEF 2005. *Standard Methods for the examination of water and wastewater*, 21st ed. American Public Health Association, Washington D.C. (USA).
- Bartzas, G., Komnitsas, K., and Paspaliaris, I. 2006. Laboratory evaluation of Fe⁰ barriers to treat acidic leachates, *Minerals Engineering*, **19**(5), 505-514.
- Bear, J. 1972. *Dynamics of Fluids in Porous Media*. American Elsevier, New York.

- Bilardi, S., Calabrò, P., and Moraci, N. 2012. Are accelerated column tests used in permeable reactive barriers design sufficiently reliable?. *In Proceedings of the third International Conference on "Hazardous and industrial waste management"*, Crete, Greece.
- Bilardi, S., Calabrò, P.S., Caré, S., Moraci, N., and Noubactep, C. 2013a. Effect of pumice and sand on the sustainability of granular iron beds for the removal of Cu^{II} , Ni^{II} , and Zn^{II} , *Clean - Soil, Air, Water*, **41**(9), 835-843.
- Bilardi, S., Calabrò, P.S., Caré, S., Moraci, N., and Noubactep, C. 2013b. Improving the sustainability of granular iron/pumice systems for water treatment. *Journal of Environmental Management*, **121**, 133-141.
- Bilardi, S., Amos, R.T., Blowes, D.W., Calabrò, P.S., and Moraci, N. 2013c. Reactive transport modelling of ZVI column experiments for nickel remediation, *Ground Water Monitoring and Remediation*, **33**(1), 97-104.
- Bilardi, S., Calabrò, P.S., and Moraci, N. 2015. Simultaneous removal of Cu^{II} , Ni^{II} and Zn^{II} by a granular mixture of zero-valent iron and pumice in column systems, *Desalination and Water Treatment*, **55**(3), 767-776.
- Calabrò, P. S., Moraci, N., and Suraci, P. 2012. Estimate of the optimum weight ratio in zero-valent iron/pumice granular mixtures used in Permeable Reactive Barriers for the Remediation of Nickel Contaminated Groundwater, *Journal of Hazardous Materials*, **207-208**, 111-116.
- Caré, S., Nguyen, Q.T., L'Hostis, V., and Berthaud, Y. 2008. Mechanical properties of the rust layer induced by impressed current method in reinforced mortar, *Cement and Concrete Research*, **38**(8-9), 1079-1091.
- Caré, S., Crane, R., Calabrò, P.S., Ghauch, A., Temgoua, E., and Noubactep, C. 2013. Modelling the permeability loss of metallic iron water filtration systems, *Clean - Soil, Air, Water*, **41**(3), 275-282.

- Carniato, L., Schoups, G., Seuntjens, P., Van Nooten, T., Simons, Q., and Bastiaens L. 2012. Predicting longevity of iron permeable reactive barriers using multiple iron deactivation models, *Journal of Contaminant Hydrology*, **142-143**, 93-108.
- Courcelles, B., Farahmand-Razavi, A.M., Gouvenot, D., and Esnault-Filet A. 2008a. Testing and Modeling the Hydraulic Permeability Evolution of Permeable Reactive Barriers Clogged by Colloids, *In Proceedings of the 12th International Conference of International Association for Computer Methods and Advances in Geomechanics (IACMAG)*, Goa, India.
- Courcelles, B., Farahmand-Razavi, A.M., Gouvenot, D., and Esnault-Filet A. 2008b. Predictive Model to Design the Permeable Reactive Barrier filters, *In Proceedings of the 12th International Conference of International Association for Computer Methods and Advances in Geomechanics (IACMAG)*, Goa, India.
- Cundy, A.B., Hopkinson, L., and Whitby, R.L.D. 2008. Use of iron-based technologies in contaminated land and groundwater remediation: A review, *Science of the Total Environment*, **400**(1-3), 42-51.
- Domga, R., Togue-Kamga, F., Noubactep C., and Tchatchuenga, J. 2015. Discussing porosity loss of Fe⁰ packed water filters at ground level, *Chemical Engineering Journal*, **263**, 127–134.
- Dries, J., Bastiaens, L., Springael, D., and Kuypers S. 2005. Effect of humic acids on heavy metal removal by zero-valent iron in batch and continuous flow column systems, *Water Research*, **39**(15), 3531–3540.
- Farrell, J., Kason, M., Melitas, N., and Li, T. 2000. Investigation of the long-term performance of zero-valent iron for reductive dechlorination of trichloroethylene. *Environmental Science & Technology*, **34**(3), 514-521.
- Fu, F., Dionysiou, D.D., and H. Liu 2014. The use of zero-valent iron for groundwater remediation and wastewater treatment: A review, *Journal of Hazardous Materials*, **267**, 194-205.

- Gu, B., Phelps, T.J., Liang, L., Dickey, M.J., Roh, Y., Kinsall, B.L., Palumbo, A.V., and Jacobs G.K. 1999. Biogeochemical dynamics in zero-valent iron columns: implications for permeable reactive barriers, *Environmental Science & Technology*, **33**(13), 2170-2177.
- Head, K.H., and Keeton, G.P. 2008. Permeability, shear strength & compressibility tests. *Manual of Soil Laboratory Testing*, vol. 2, Whittles Publishing, United Kingdom.
- Henderson, A.D. 2004. Solids Formation and Permeability Reduction in Zero-Valent Iron and Iron Sulfide Media for Permeable Reactive Barriers, Dissertation submitted in partial fulfillment of the requirements for the degree of Doctor of Philosophy (Environmental Engineering), University of Michigan.
- Henderson, A.D., and Demond, A.H. 2007. Long-Term Performance of Zero-Valent Iron Permeable Reactive Barriers: A Critical Review. *Environmental Engineering Science*, **24**(4), 401-423.
- Henderson, A.D., and Demond, A.H. 2011. Impact of solids formation and gas production on the permeability of ZVI PRBs, *Journal of Environmental Engineering*, **137**(8), 689-696.
- Henderson, A.D., and Demond, A.H. 2013. Permeability of iron sulfide (FeS)-based materials for groundwater remediation, *Water Research*, **47**(3), 1267-1276.
- Interstate Technology & Regulatory Council (ITRC) 2011. *Permeable Reactive Barrier: Technology Update*, Washington, DC.
- Jeen S-W., Gillham, R.W., and Blowes, D.W. 2006. Effects of Carbonate Precipitates on Long-Term Performance of Granular Iron for Reductive Dechlorination of TCE. *Environmental Science & Technology*, **40**, 6432-6437.
- Jeen, S-W., Gillham, R.W., and Przepiora, A. 2011. Predictions of long-term performance of granular iron permeable reactive barriers: Field-scale evaluation, *Journal of Contaminant Hydrology*, **123**(1-2), 50-64.

- Jeen, S-W., Amos, R.T., and Blowes, D.W. 2012. Modelling gas formation and mineral precipitation in a granular iron column, *Environmental Science & Technology*, **46**(12), 6742-6749.
- Kamolpornwijit, W., Liang, L., West, O.R., Moline, G.R., and Sullivan, A.B. 2003. Preferential flow path development and its influence on long-term PRB performance: Column study, *Journal of Contaminant Hydrology*, **66**(3-4), 161– 178.
- Kamolpornwijit, W., and Liang, L. 2006. Investigation of gas production and entrapment in granular iron medium, *Journal of Contaminant Hydrology*, **82**(3-4), 338– 356.
- Kaplan, D.I., Gilmore, T.J., 2004. Zero-valent iron removal rates of aqueous Cr(VI) measured under flow conditions. *Water, Air, & Soil Pollution*, **155**, 21-33.
- Komnitsas, K., Bartzas, G., and Paspaliaris, I. 2006. Inorganic contaminant fate assessment in zero-valent iron treatment walls, *Environmental forensics*, **7**(3), 207-217.
- Li, L., Benson, C.H., and Lawson, E.M. 2005. Impact of mineral fouling on hydraulic behaviour of permeable reactive barriers, *Ground Water*, **43**(4), 582-596.
- Li, L., Benson, C.H., and Lawson, E.M. 2006. Modeling porosity reductions caused by mineral fouling in continuous-wall permeable reactive barriers, *Journal of Contaminant Hydrology*, **83**(1-2), 89-121.
- Liang, L.Y., Korte, N.E., Gu, B., Puls, R., and Reeter, C. 2000. Geochemical and microbial reactions affecting the long-term performance of in situ 'iron barriers', *Advances in Environmental Research*, **4**(4), 273-286.
- Mackenzie, P.D., Horney, D.P., and Sivavec, T.M. 1999. Mineral precipitation and porosity losses in granular iron columns, *Journal of Hazardous Materials*, **68**(1-2), 1-17.
- Moraci, N., 2010. Geotextile filter: Design, characterization and factors affecting clogging and blinding limit states, 9th International Conference on Geosynthetics - Geosynthetics: Advanced Solutions for a Challenging World, Guarujá, Brazil, 23 - 27 May 2010, pp. 413-438.

- Moraci, N., and Calabrò, P.S. 2010. Heavy Metals Removal and Hydraulic Performance in Zero-Valent Iron/Pumice Permeable Reactive Barriers, *Journal of Environmental Management.*, **91**(11), 2336-2341.
- Moraci, N., Calabrò, P.S., and Suraci, P. 2011. Long-term efficiency of Zero-Valent Iron - Pumice granular mixtures for the removal of Copper or Nickel from groundwater, *Soils and Rocks*, **34**(2), 129-137.
- Moraci, N., Mandaglio, M.C., and Ielo, D. 2012a. A new theoretical method to evaluate the internal stability of granular soil, *Canadian Geotechnical Journal*, **49**(1), 45-58.
- Moraci, N., Mandaglio, M.C., and Ielo, D. 2012b. Reply to the discussion by Dallo and Wang on “A new theoretical method to evaluate the internal stability of granular soils”, *Canadian Geotechnical Journal*, **49**(7), 866-868.
- Moraci, N., Ielo, D., and Mandaglio, M.C. 2012c. A new theoretical method to evaluate the upper limit of the retention ratio for the design of geotextile filters in contact with broadly granular soils, *Geotextiles and Geomembranes* **35**, 50-60.
- Moraci, N., Bilardi, S., and Calabrò, P.S. 2014a. Critical aspects related to Fe⁰ and Fe⁰/pumice PRB design, *Environmental Geotechnics*, doi: 10.1680/envgeo.13.00120.
- Moraci, N., Mandaglio, M.C., and Ielo, D. 2014b. Analysis of the internal stability of granular soils using different methods, *Canadian Geotechnical Journal*, **51**(9), 1063-1072.
- Moraci, N., Bilardi, S., and Calabrò, P.S. 2015a. Progettazione Di Barriere Permeabili Reattive Per La Bonifica Di Acquiferi Contaminati Da Metalli Pesanti. (Design Of Permeable Reactive Barriers For Remediation Of Groundwater Contaminated By Heavy Metals), *Rivista Italiana di Geotecnica*, **49**(2), 59-86.
- Moraci, N., Mandaglio, M.C., and Ielo, D. 2015b. Reply to the discussion by Ni et al. on “Analysis of the internal stability of granular soils using different methods, *Canadian Geotechnical Journal*, **52**(3), 385-391.

- Musso, A., and Federico, F. 1983. A geometric probabilistic method to verify filter stability, *Rivista Italiana di Geotecnica*, 177-193.
- Noubactep, C. 2010. Metallic iron for safe drinking water worldwide, *Chemical Engineering Journal*, **165**(2), 740-749.
- Noubactep, C. 2011. Aqueous contaminant removal by metallic iron: is the paradigm shifting? *Water SA*, **37**(3), 419-426.
- Noubactep, C., 2013. On the suitability of admixing sand to metallic iron for water treatment. *International Journal of Environmental Pollution and Solutions*, **1**, 22-36.
- O, J.S., Jeon, S.W, Gillham, R.W., and Gui, L. 2009. Effect of initial corrosion rate on long-term performance of iron reactive barriers: Column experiments and numerical simulation, *Journal of Contaminant Hydrology*, **103**(3-4), 145-156.
- Parbs, A., Ebert, M., and Dahmke, A. 2007. Long-term effects of dissolved carbonate species on the degradation of trichloroethylene by zerovalent iron. *Environmental Science & Technology*, **41**(1): 291-296
- Pilling, N.B., and Bedworth, R.E. 1923. The oxidation of metals at high temperatures. *Journal of the Institute of Metals*, **29**, 529-591.
- Rangsivek, R., and Jekel, M.R. 2005. Removal of dissolved metals by zero-valent iron (ZVI): kinetics, equilibria, processes and implications for stormwater runoff treatment, *Water Research*, **39**(17), 4153-4163.
- Rangsivek, R., and Jekel M.R., 2011. Development of an on-site Fe⁰ system for treatment of copper- and zinc-contaminated roof runoff, *International Journal of Environment and Waste Management*, **8**(3-4), 353-365.
- Reardon, E.J. 1995. Anaerobic corrosion of granular iron: measurement and interpretation of hydrogen evolution rates, *Environmental Science & Technology*, **29**(12), 2936-2945.
- Reardon, E.J. 2005. Zero valent Irons: Styles of Corrosion and Inorganic Control on Hydrogen Pressure Buildup, *Environmental Science & Technology*, **39**(18), 7311-7317.

- Repta, C.J.W., 2001. Evaluation of nickel-enhanced granular iron for the dechlorination of trichlorethene, M.Sc. thesis, Dep. of Earth Sciences, University of Waterloo, Waterloo, Ontario.
- Ruhl, A.S., Weber, A., and Jekel, M. 2012a. Influence of dissolved inorganic carbon and calcium on gas formation and accumulation in iron permeable reactive barriers, *Journal of Contaminant Hydrology*, **142–143**, 22-32.
- Ruhl, A.S., Ünal, N., and Jekel, M. 2012b. Evaluation of two-component Fe(0) fixed bed filters with porous materials for reductive dechlorination, *Chemical Engineering Journal*, 209, 401-406.
- Silveira, A. 1965. An analysis of the problem of washing through in protective filters, In *Proceedings of the 6th ICSMFE*, Montreal, Canada.
- Silveira, A., Jr J. De Lorena Peixoto, and Noguetera, J.B. 1975. On void-size distribution of granular materials, 5th Panamerican conference on soil mechanics and foundation engineering, Buenos Aires, Argentina, **3**, 161-177.
- Triszcz, J.M., Porta, A. and García Einschlag, F.S. 2009. Effect of operating conditions on iron corrosion rates in zero-valent iron systems for arsenic removal. *Chemical Engineering Journal*, **150**, 431–439.
- Wilkin, R.T., Puls, R.W., and Sewell, G.W. 2003. Long-term performance of permeable reactive barriers using zero-valent iron: geochemical and microbiological effects *Ground Water*, **41**, 493–503.
- Velimirovic, M., Carniato, L., Simons, Q., Schoups, G., Seuntjens, P. and Bastiaens L. 2014. Corrosion rate estimations of microscale zerovalent iron particles via direct hydrogen production measurements. *Journal of Hazardous Materials*, **270**, 18–26
- Zhang, Y., and Gillham, R. W. 2005. Effects of gas generation and precipitates on performance of Fe⁰ PRBs. *Ground Water*, **43**(1), 113-121.

Zhao, Y., Ren, H., Dai, H., and Jin, W. 2011. Composition and expansion coefficient of rust based on X-ray diffraction and thermal analysis, *Corrosion Science*, **53**(5), 1646–1658.

Draft

FIGURES CAPTIONS

Figure 1. Zero valent iron grain size distribution

Figure 2. Reactive medium schematization as “s” layers of dimensions “n·m”

Figure 3. Discretization of grain size distribution according to Silveira (1965) method.

Figure 4. Set *i*-th of 4 particles and set *i*-th equivalent with constriction size.

Figure 5. Grain size distribution in mass, in number and constrictions size distribution.

Figure 6. Random choice of a bubble or constriction. X, value of the bubble diameter or of the soil constriction included in the layer

Figure 7. Scheme of comparison between bubbles and constrictions

Figure 8. Schematization of bubbles blocked and passing

Figure 9. Set *i*-th of 4 particles of diameter D_{mean} and volume and surface overlapping

Figure 10. Two different methods taken into account for modelling the formation of precipitates.

Figure 11. Constriction variation due to precipitates

Figure 12. Experimental data and model results of the ratio k/k_0 as function of time for column test A using a) simulation approach 1 and b) simulation approach 2.

Figure 13. Experimental data and model results of the ratio k/k_0 as function of time for column test B using a) simulation approach 1 and b) simulation approach 2.

Figure 14. Experimental data and model results of the ratio k/k_0 as function of time for column test C using a) simulation approach 1 and b) simulation approach 2.

Figure 15. Experimental data and model results of the ratio k/k_0 as function of time for column test D using a) simulation approach 1 and b) simulation approach 2.

Figure 16. Experimental data and model results of the ratio k/k_0 as function of time for column test E using a) simulation approach 1 and b) simulation approach 2.

Figure 17. Experimental data and model results of the ratio k/k_0 as function of time for column test F using a) simulation approach 1 and b) simulation approach 2.

Figure 18. Experimental data and model results of the ratio k/k_0 as function of time for column test G using a) simulation approach 1 and b) simulation approach 2.

Figure 19. Variation of the porosity loss (%) due to ZVI expansion and mineral precipitation as function of α in absence of H_2 using the simulation approach 2.

Draft

Table 1. Column test conditions

ID	Contaminant	Contaminant concentration [mg/l]	Flow rate [ml/min]	Darcy velocity [m/day]	Mass of ZVI [g]	Thickness [cm]
A	Ni	40	0.1	0.07	1680	22.5
B	Ni	40	2.5	1.9	1680	22.5
C	Ni	50	0.5	0.38	240	3
D	Ni	8	0.1	0.07	240	3
E	Ni, Cu, Zn	50, 500, 50	0.5	0.38	240	3
F	Ni	8	2.5	1.9	1680	22.5
G	Ni	95	2.5	1.9	1680	22.5

Table 2: Input parameters used in both simulation approaches 1 and 2.

Parameter	value
Volumes of precipitates at the end of the test calculated at 1.5 or 3 cm from column inlet	406 mm ³ (test A – 3 cm) 245mm ³ (test B – 1.5 cm) 156 mm ³ (test C – 1.5 cm) 56 mm ³ (test D – 3 cm) 1084 mm ³ (test E – 3 cm) 73 mm ³ (test F – 1.5 cm) 241 mm ³ (test G – 1.5 cm)
Layer schematization	30 layer x 30 rows x 30 columns
Expansion coefficient η	2.37 (all Test)
Test column duration	9000 h (Test A) 856 h (Test B) 1200 h (Test C) 6000 h (Test D) 600 h (Test E) 432 h (Test F) 657 h (Test G)

Table 3: Calibration parameters in the simulation approach 1.

Parameter	Value
Iron corrosion rate	0.7 mmol/kg*d (Test A) 10 mmol/kg*d (Test B) 1.5 mmol/kg*d (Test C) 1.2 mmol/kg*d (Test D) 4 mmol/kg*d (Test E) 12 mmol/kg*d (Test F) 7 mmol/kg*d (Test G)
Average gas bubbles diameter	0.167 (Test A) 0.17 (Test B)

μ [mm]	0.165 (Test C)
	0.175 (Test D)
	0.193 (Test E)
	0.17 (Test F)
	0.17 (Test G)
Standard deviation of gas bubbles diameter frequency distribution	0.003 (Test A)
	0.008 (Test B)
σ [mm]	0.001 (Test C)
	0.01 (Test D)
	0.009 (Test E)
	0.012 (Test F)
	0.012 (Test G)

Table 4: Calibration parameters in the simulation approach 2.

Parameter	Value
Iron corrosion rate	21 mmol/kg*d (Test A)
	200 mmol/kg*d (Test B)
	15 mmol/kg*d (Test C)
	30 mmol/kg*d (Test D)
	242 mmol/kg*d (Test E)
	300 mmol/kg*d (Test F)
	170 mmol/kg*d (Test G)

Table 5: Porosity loss (%) due to ZVI expansion and mineral precipitation and extent of ZVI depletion α in presence of H_2 (simulation approach 1) and considering its absence (simulation approach 2).

Test	H_2 (simulation approach 1)		H_2 absence (simulation approach 2)	
	Porosity loss [%]	α [%]	Porosity loss [%]	α [%]
A	4.8	1.46	98	43.9
B	7.2	1.99	99.6	39.8
C	2.2	0.42	12	4.2
D	4.6	1.67	99	41.8
E	5.4	0.56	93.2	33.7
F	3.7	1.20	80	30.1
G	4.7	1.07	70.5	26.0

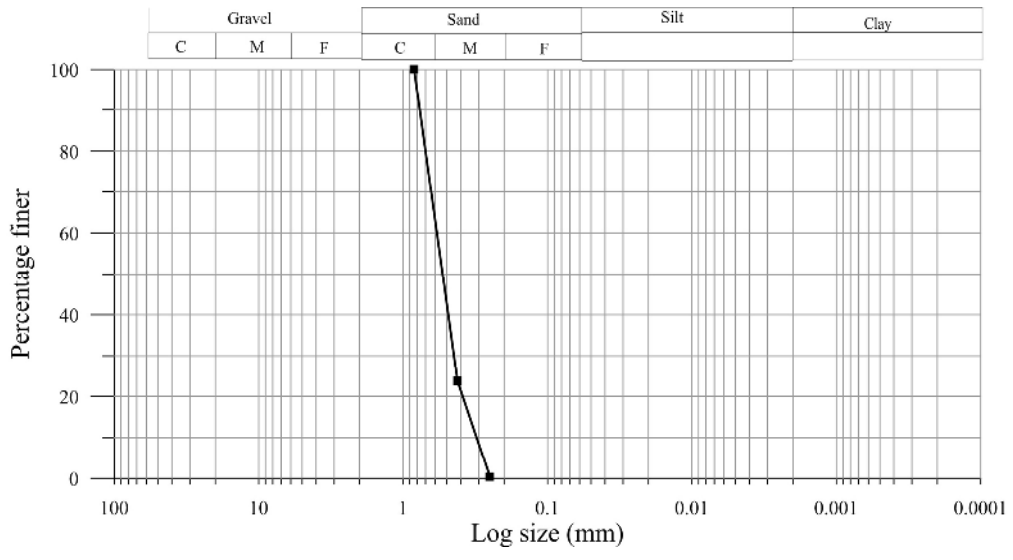


Figure 1. Zero valent iron grain size distribution
181x98mm (299 x 299 DPI)

Draft

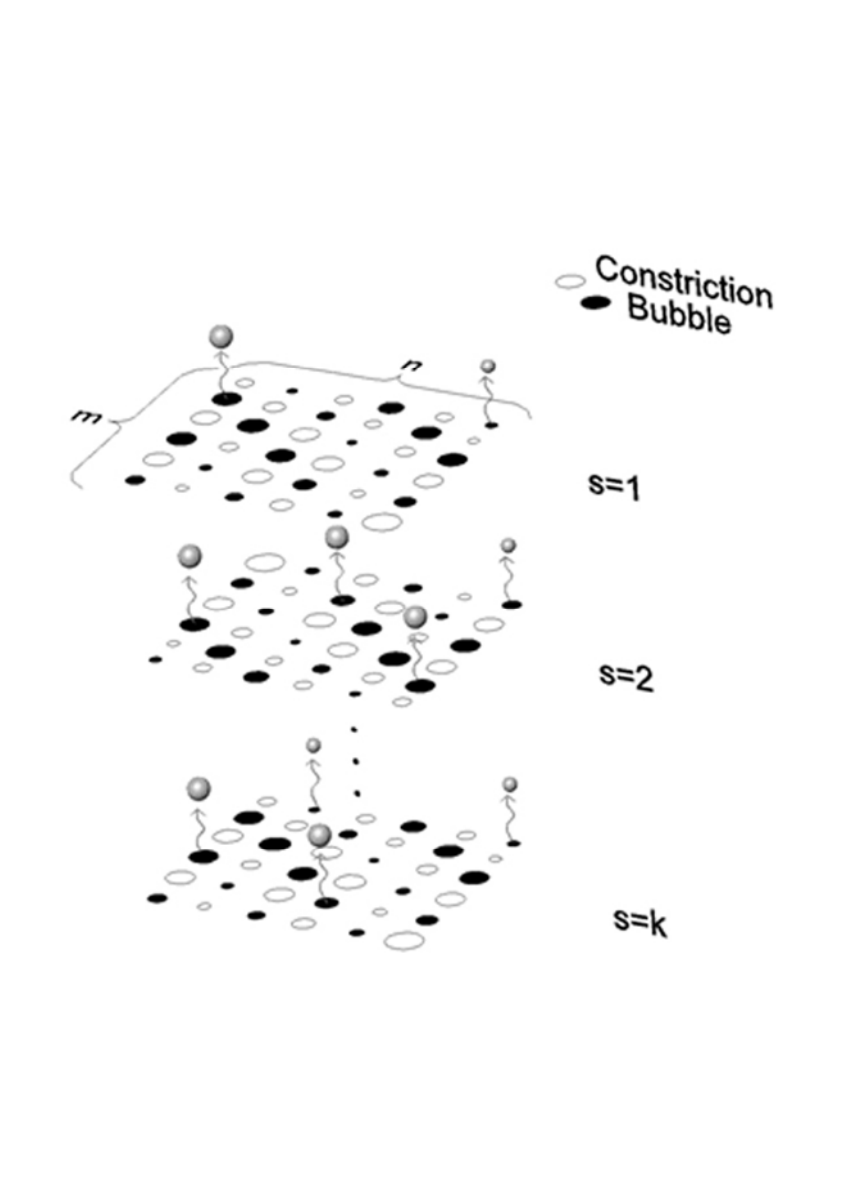


Figure 2. Reactive medium schematization as " s " layers of dimensions " $n \cdot m$ "
82x116mm (200 x 200 DPI)

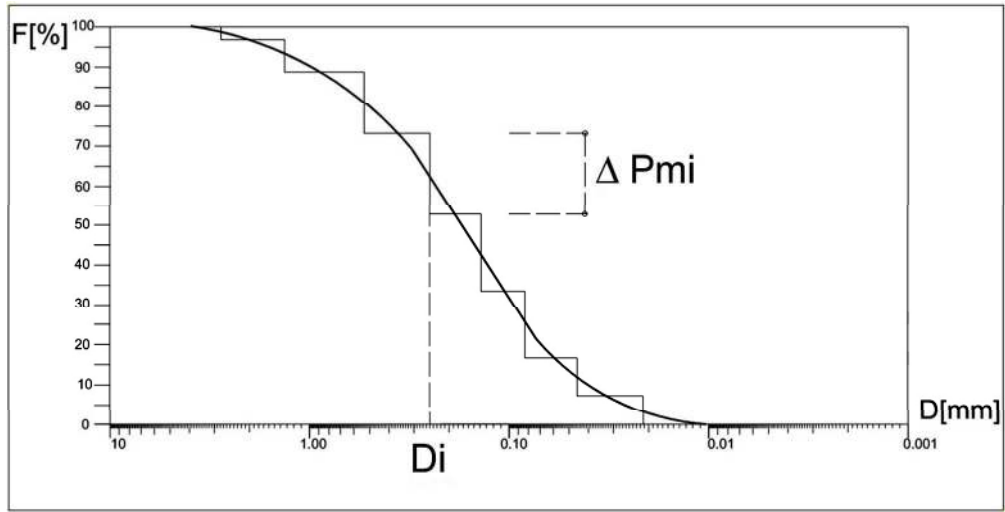


Figure 3. Discretization of grain size distribution according to Silveira (1965) method. 181x92mm (220 x 220 DPI)

Draft

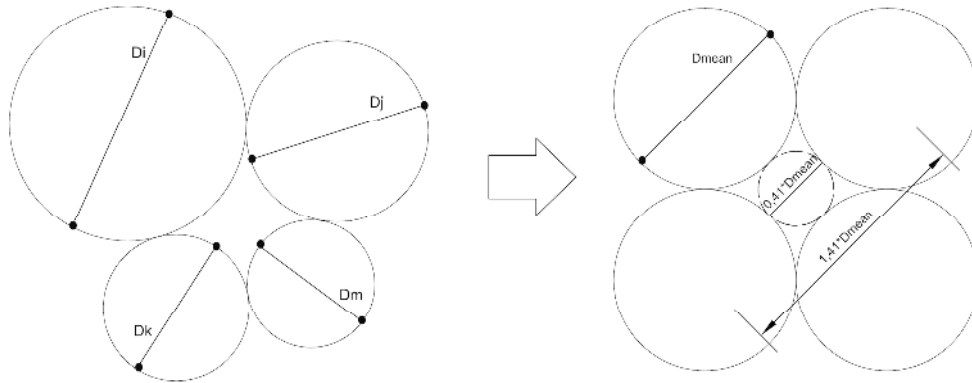


Figure 4. Set i -th of 4 particles and set i -th equivalent with constriction size.
182x87mm (300 x 300 DPI)

Draft

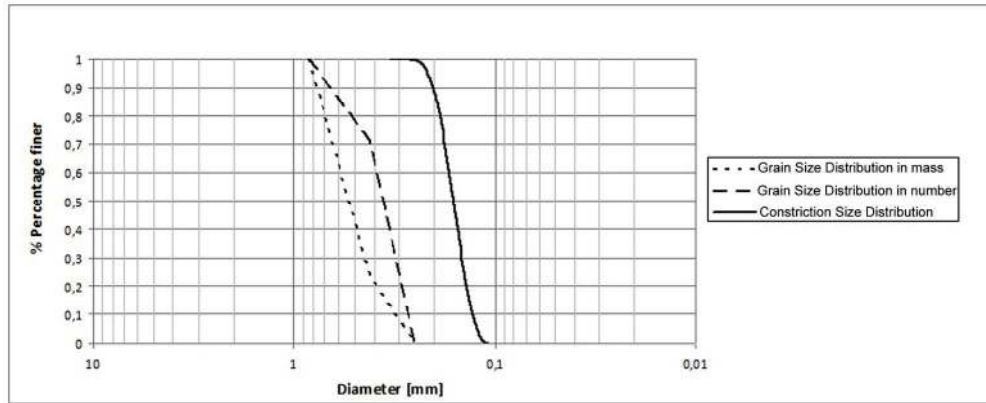


Figure 5. Grain size distribution in mass, in number and constrictions size distribution.
181x74mm (250 x 250 DPI)

Draft

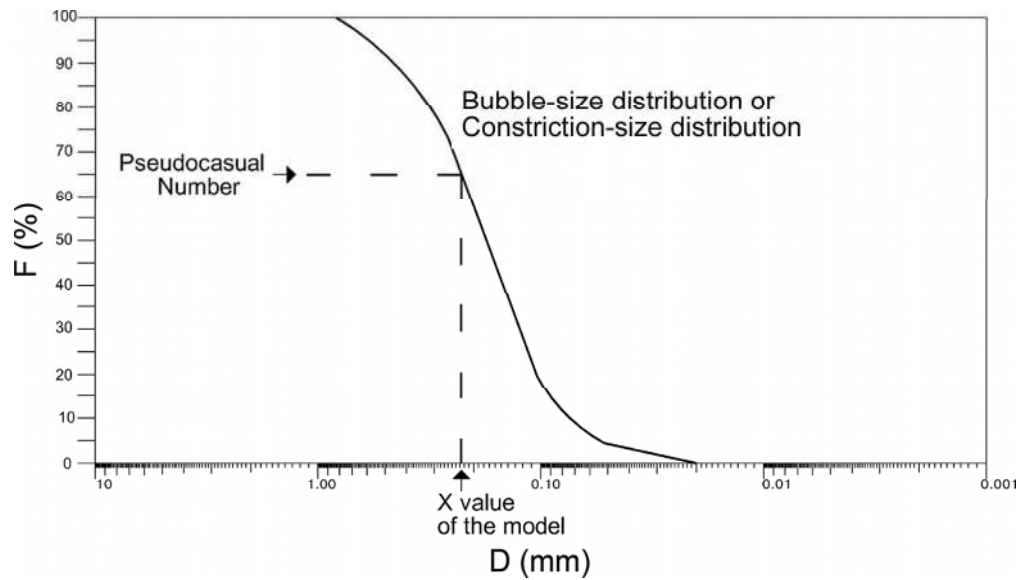


Figure 6. Random choice of a bubble or constriction. X , value of the bubble diameter or of the soil constriction included in the layer
181x102mm (250 x 250 DPI)

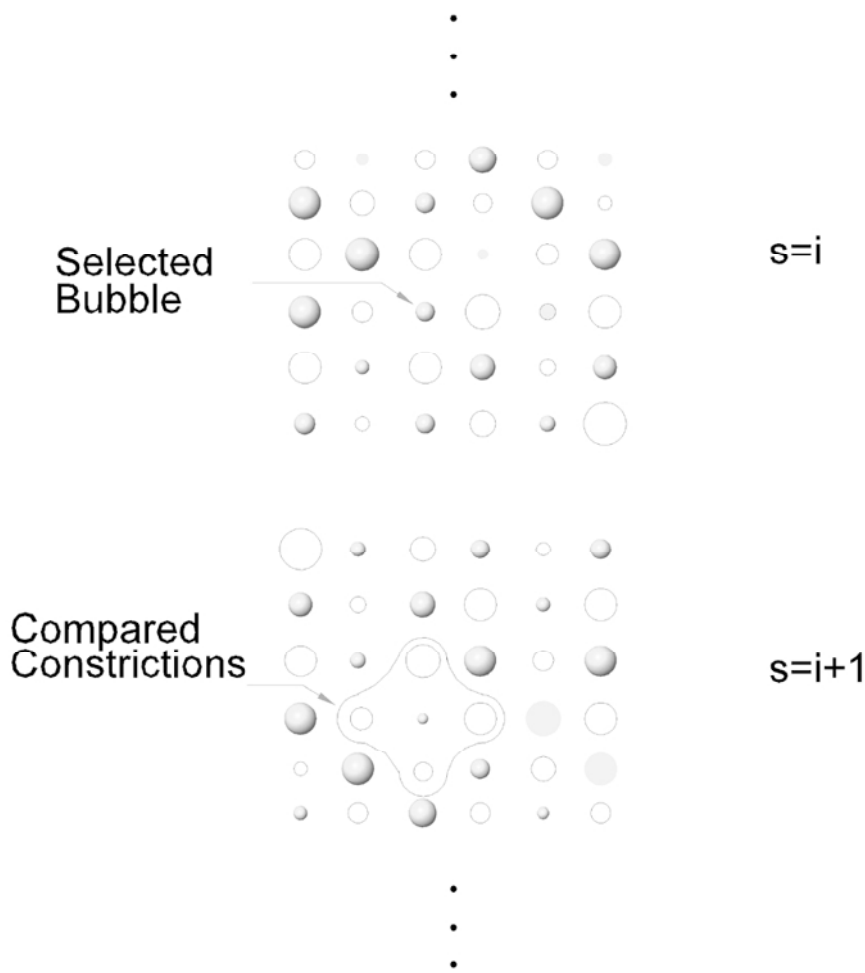


Figure 7. Scheme of comparison between bubbles and constrictions
82x89mm (300 x 300 DPI)

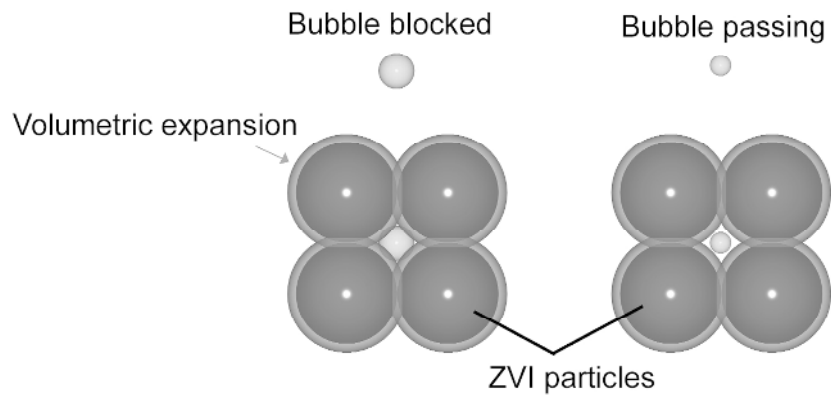


Figure 8. Schematization of bubbles blocked and passing
182x79mm (300 x 300 DPI)

Draft

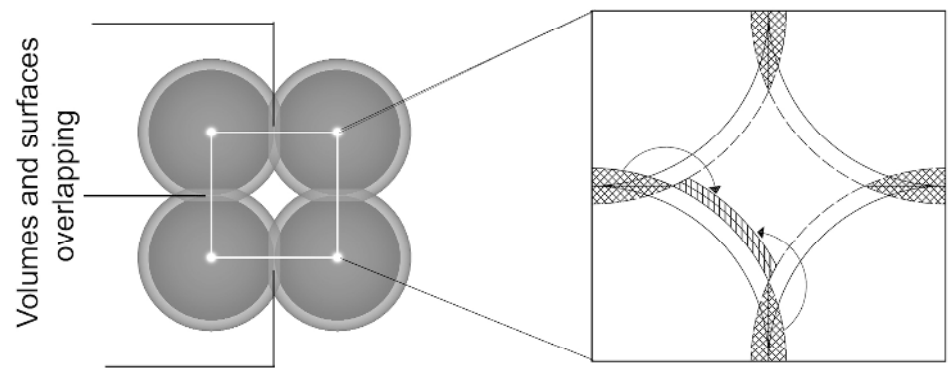


Figure 9. Set i -th of 4 particles of diameter D_{mean} and volume and surface overlapping
182x97mm (300 x 300 DPI)

Draft

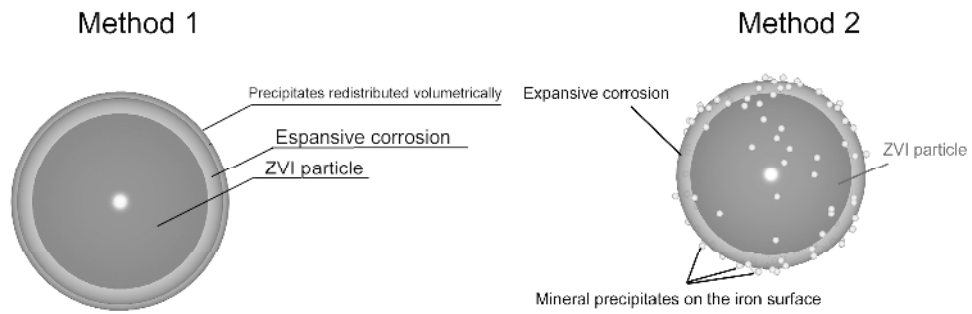
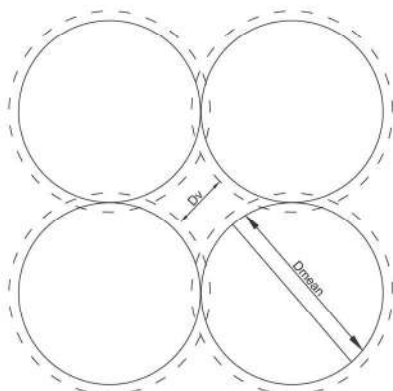


Figure 10. Two different methods taken into account for modelling the formation of precipitates
956x322mm (72 x 72 DPI)

Draft

With mineral precipitate volume redistributed



With mineral precipitate particles

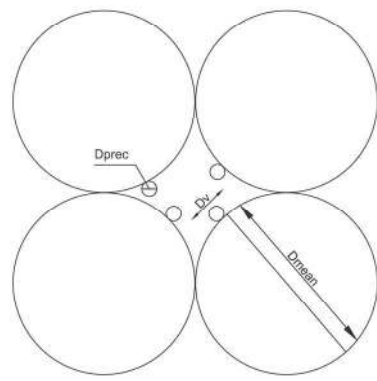


Figure 11. Constriction variation due to precipitates
182x83mm (300 x 300 DPI)

Draft

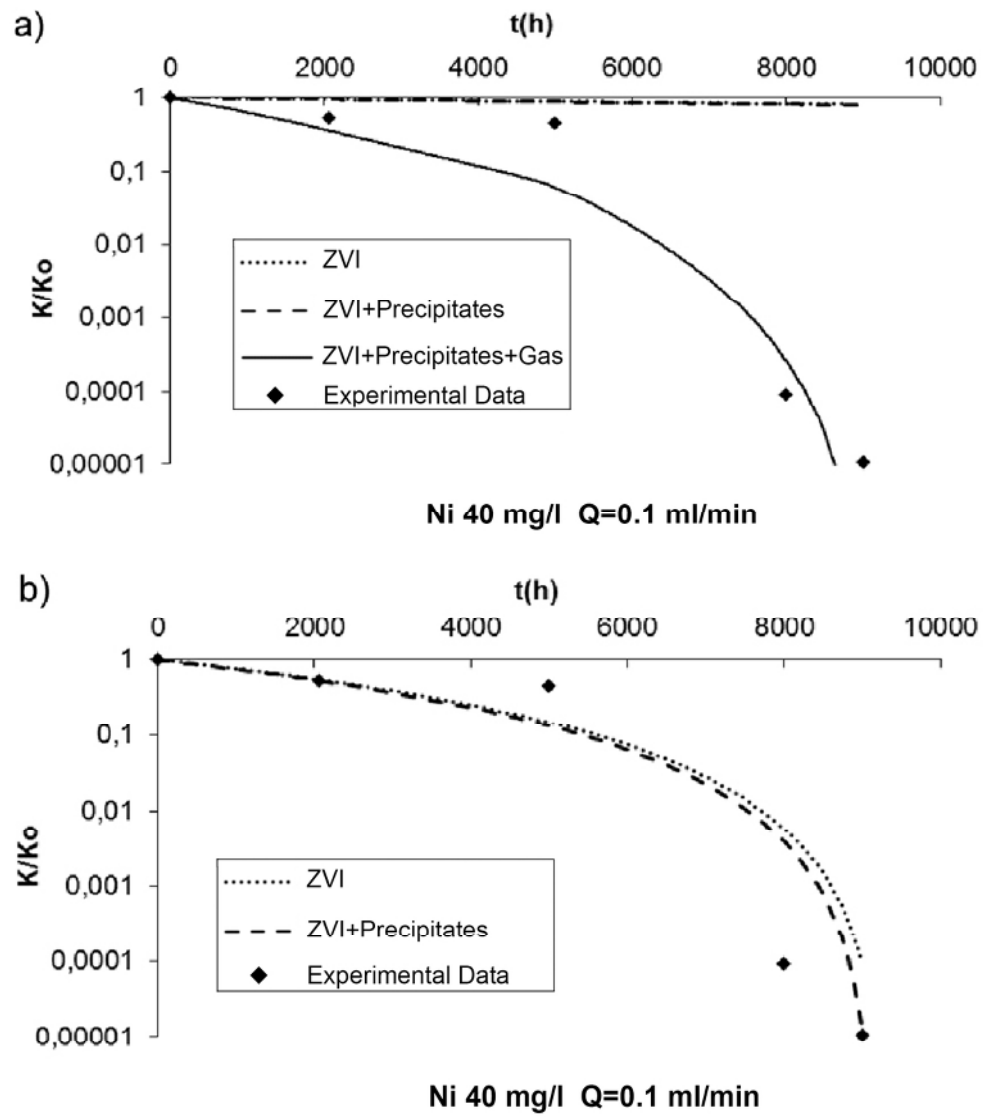


Figure 12. Experimental data and model results of the ratio k/k_0 as function of time for column test A using
 a) simulation approach 1 and b) simulation approach 2
 99x116mm (300 x 300 DPI)

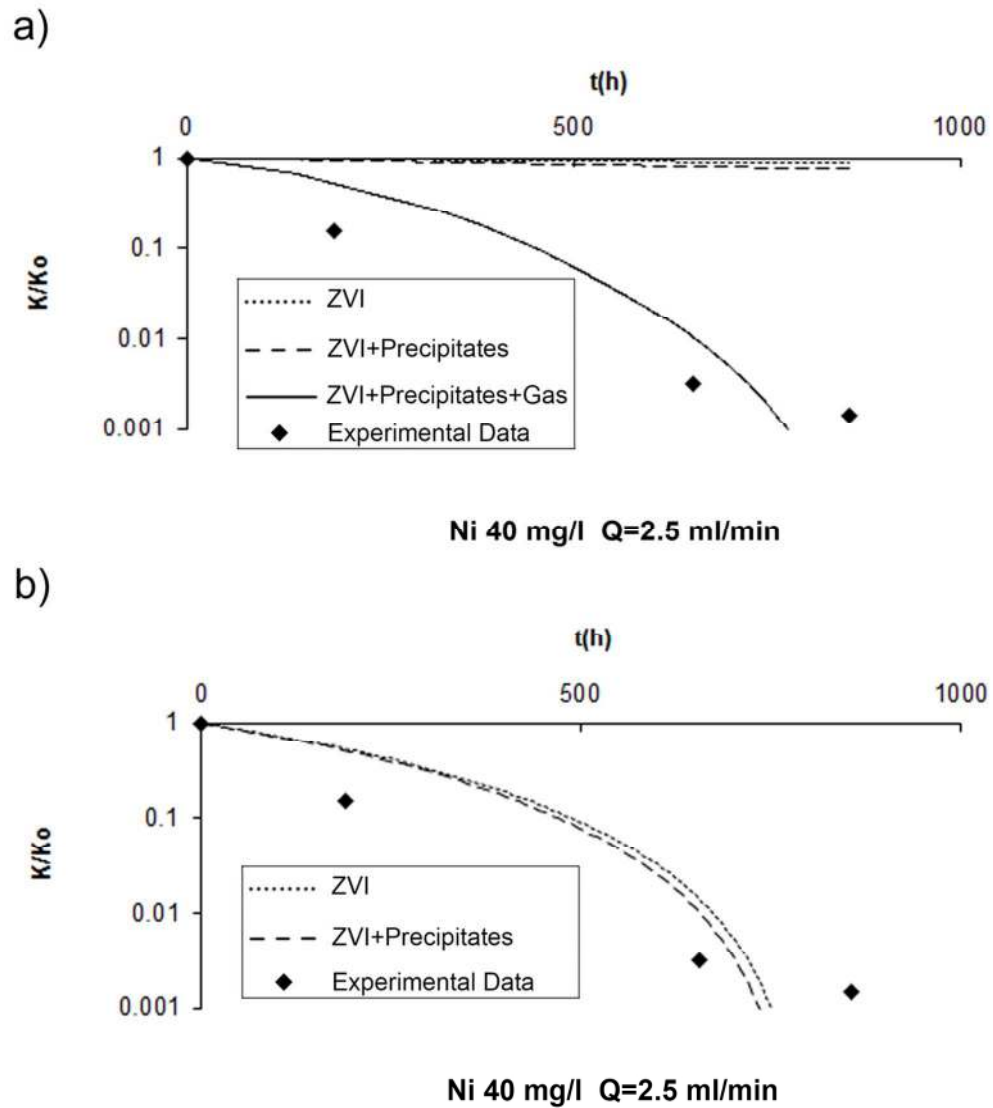


Figure 13. Experimental data and model results of the ratio k/k_0 as function of time for column test B using
 a) simulation approach 1 and b) simulation approach 2
 99x116mm (300 x 300 DPI)

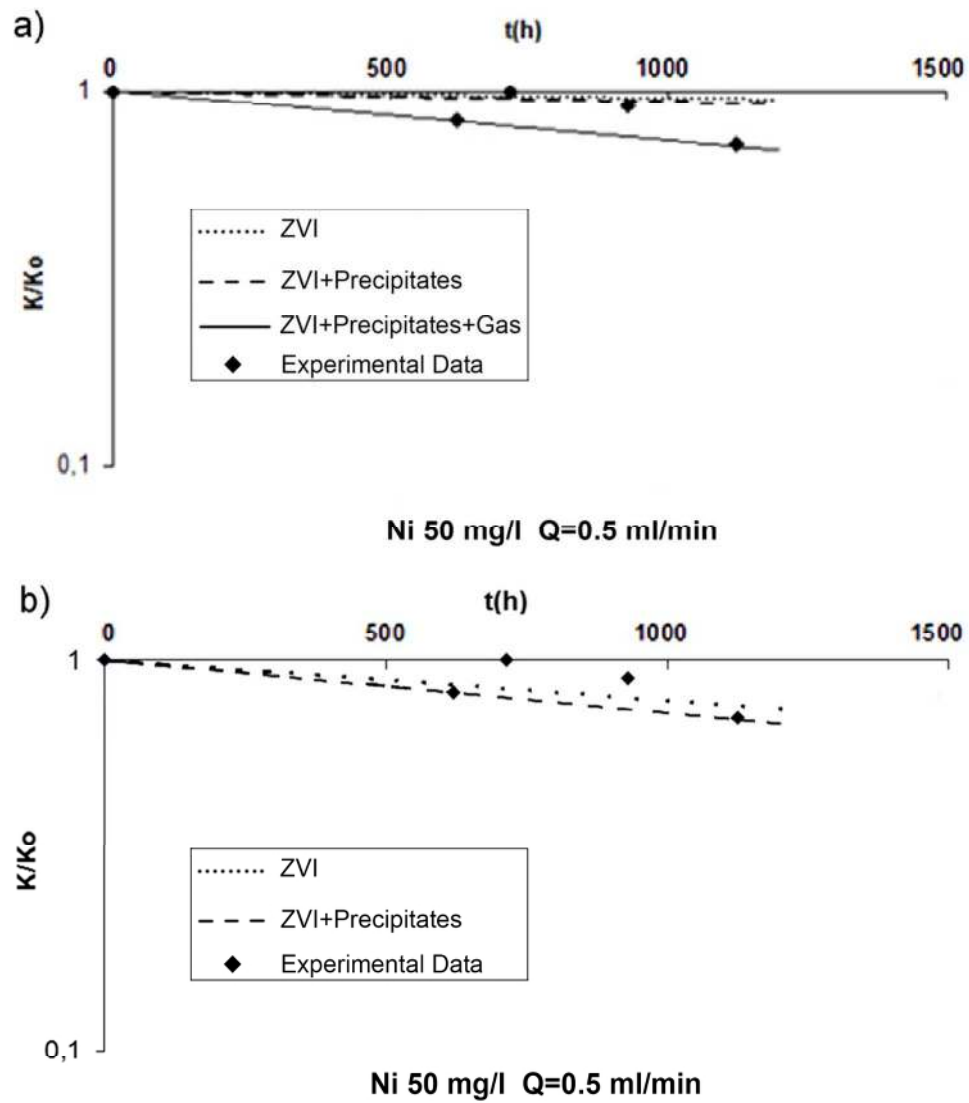


Figure 14. Experimental data and model results of the ratio k/k_0 as function of time for column test C using
 a) simulation approach 1 and b) simulation approach 2
 99x116mm (300 x 300 DPI)

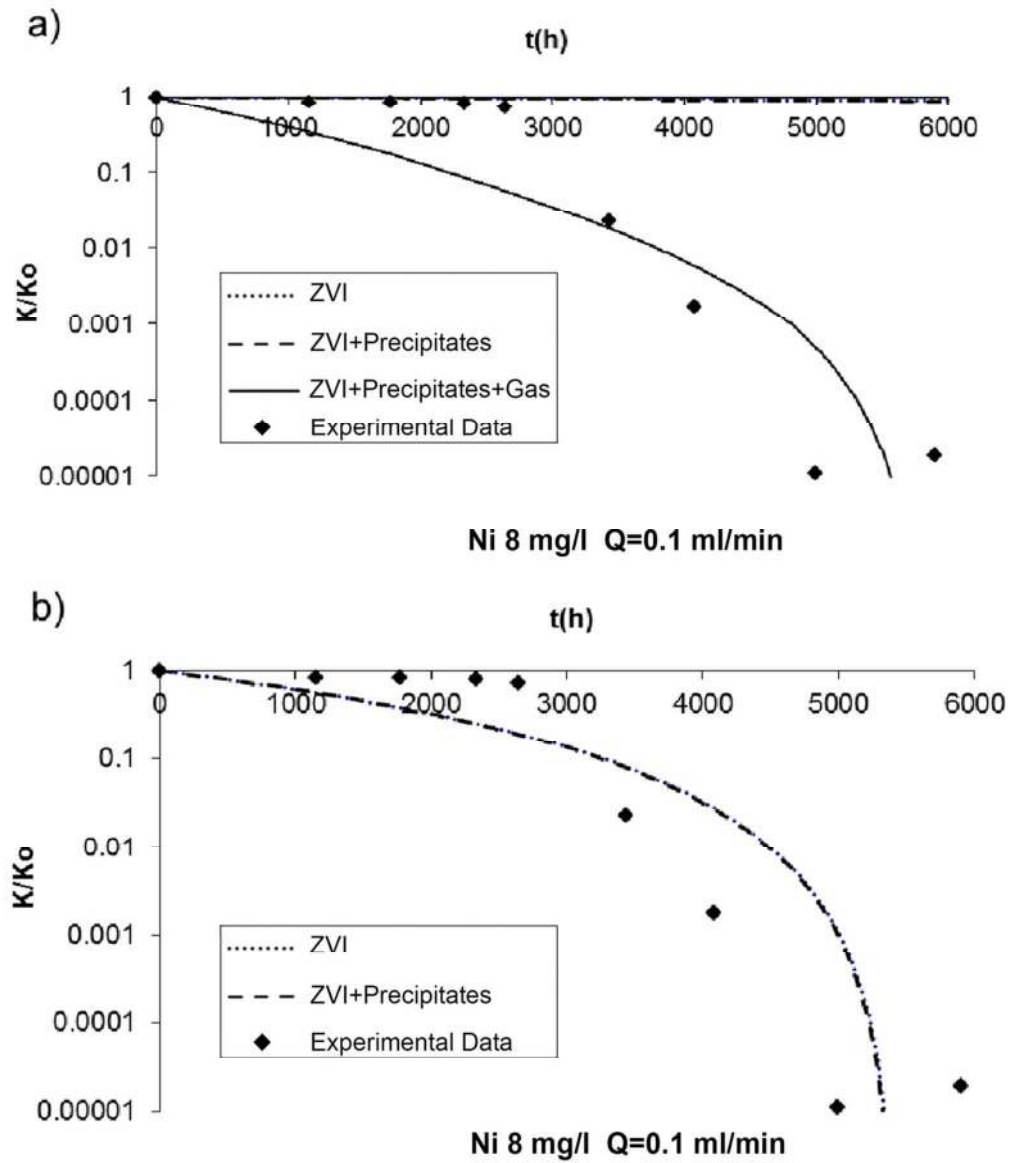


Figure 15. Experimental data and model results of the ratio k/k_0 as function of time for column test D using
 a) simulation approach 1 and b) simulation approach 2
 99x116mm (300 x 300 DPI)

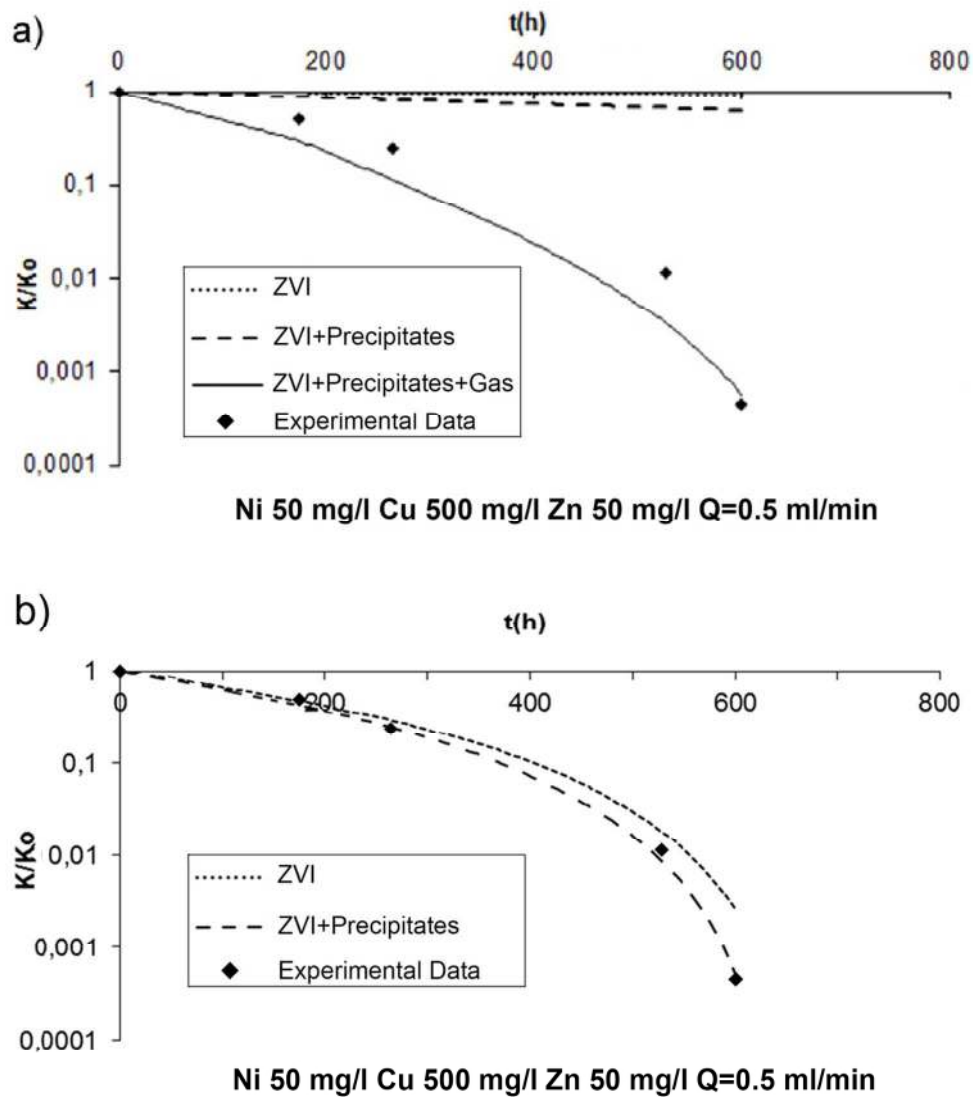


Figure 16. Experimental data and model results of the ratio k/k_0 as function of time for column test E using
 a) simulation approach 1 and b) simulation approach 2
 99x116mm (300 x 300 DPI)

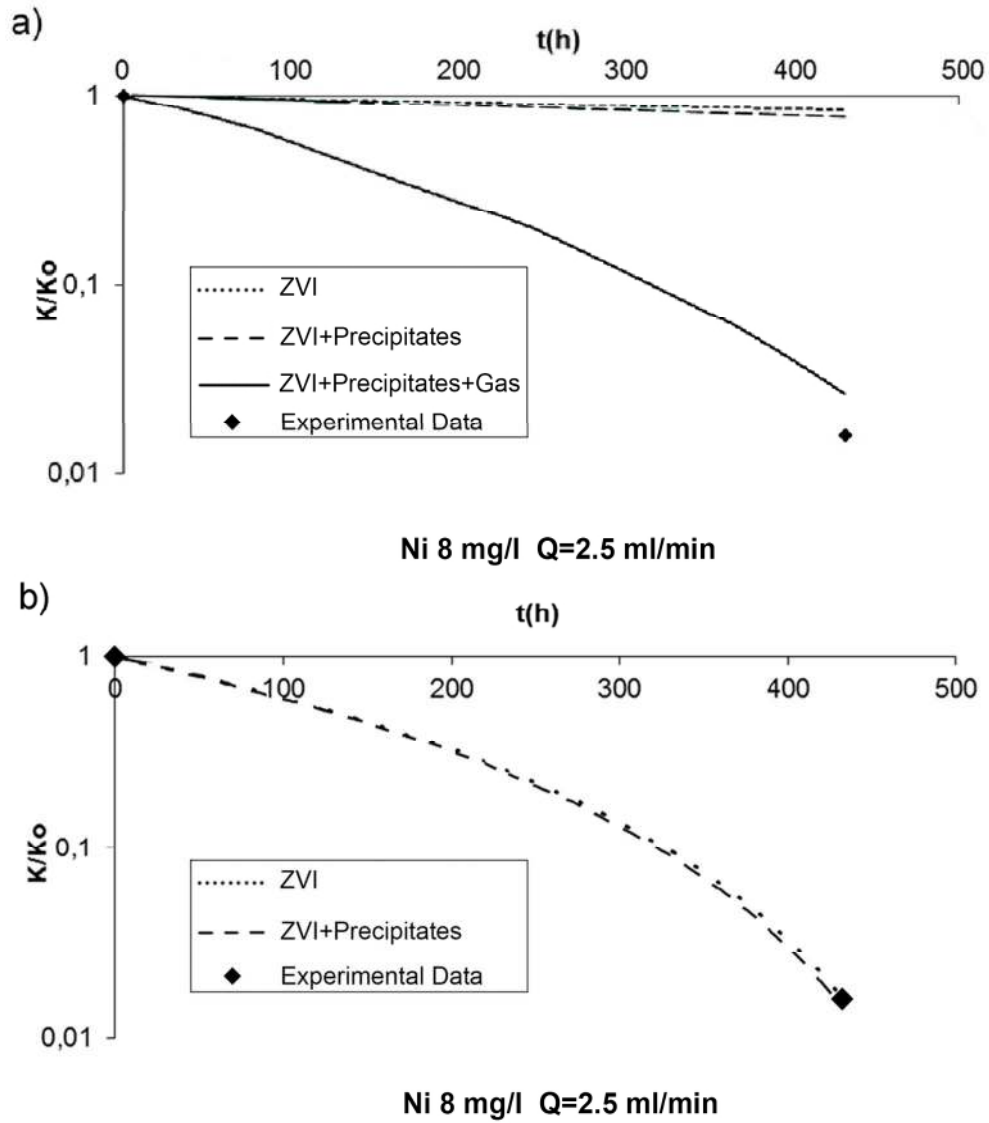


Figure 17. Experimental data and model results of the ratio k/k_0 as function of time for column test F using a) simulation approach 1 and b) simulation approach 2
99x116mm (300 x 300 DPI)

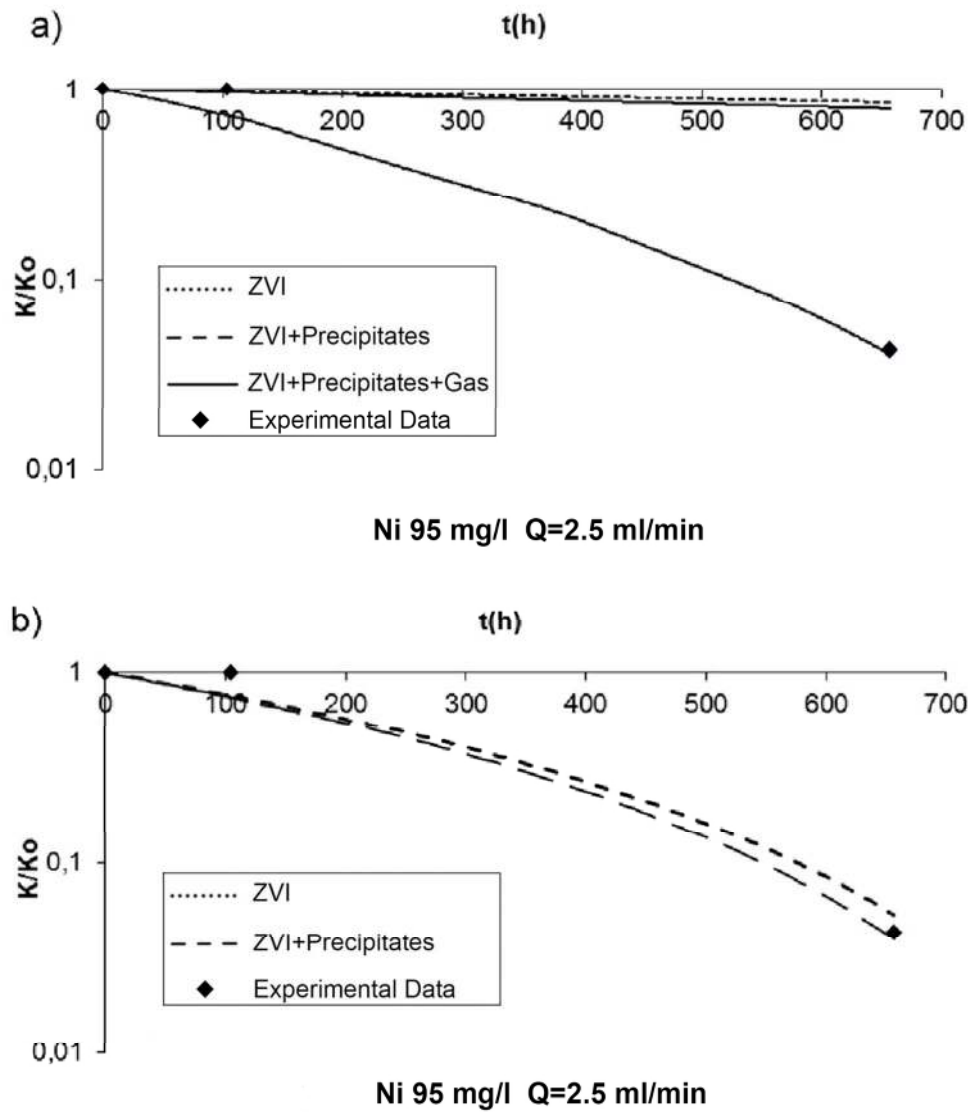


Figure 18. Experimental data and model results of the ratio k/k_0 as function of time for column test G using a) simulation approach 1 and b) simulation approach 2
99x116mm (300 x 300 DPI)

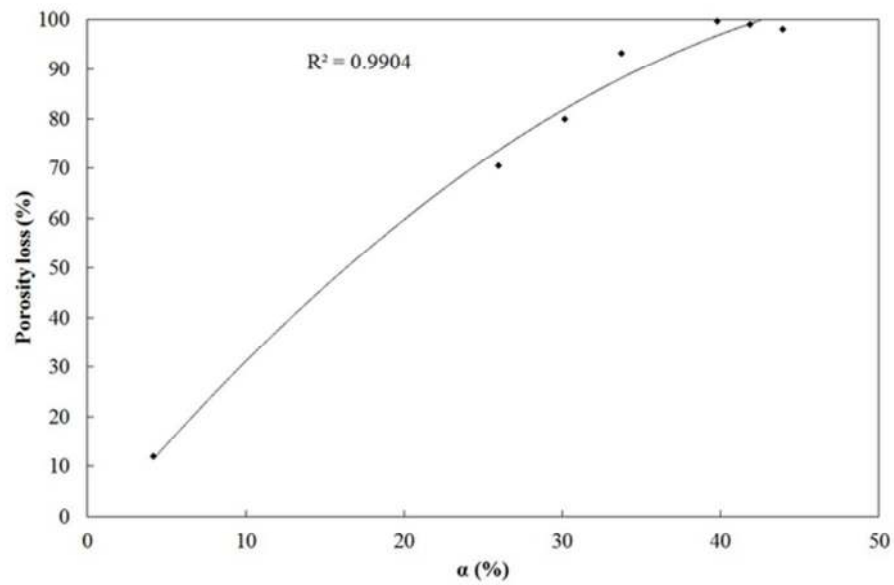


Figure 19. Variation of the porosity loss (%) due to ZVI expansion and mineral precipitation as function of α in absence of H₂ using the simulation approach 2
56x36mm (300 x 300 DPI)